Colloids and Surfaces A: Physicochemical and Engineering Aspects 688 (2024) 133528

Contents lists available at ScienceDirect

Colloids and Surfaces A: Physicochemical and Engineering Aspects

journal homepage: www.elsevier.com/locate/colsurfa

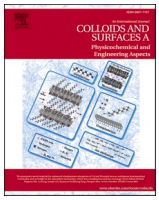

Preparation, characterization and in vitro evaluation of the antimicrobial and antitumor activity of MnOx nanoparticles

Andrea Rónavári [a,1], Altantuya Ochirkhuyag [a,b,1], Nóra Igaz [c], Bettina Szerencsés [d], Gergő Ballai [a], Ildikó Huliák [c], Csenge Bocz [c], Ákos Kovács [c], Ilona Pfeiffer [d], Mónika Kiricsi [c,*,1], Zoltán Kónya [a,e,1]

[a] Department of Applied and Environmental Chemistry, University of Szeged, Szeged, Hungary
[b] Laboratory of Material Science and Technology, Institute of Chemistry and Chemical Technology, Mongolian Academy of Sciences, Ulaanbaatar, Mongolia
[c] Department of Biochemistry and Molecular Biology, University of Szeged, Szeged, Hungary
[d] Department of Microbiology, University of Szeged, Szeged, Hungary
[e] ELKH-SZTE Reaction Kinetics and Surface Chemistry Research Group, Szeged, Hungary

GRAPHICAL ABSTRACT

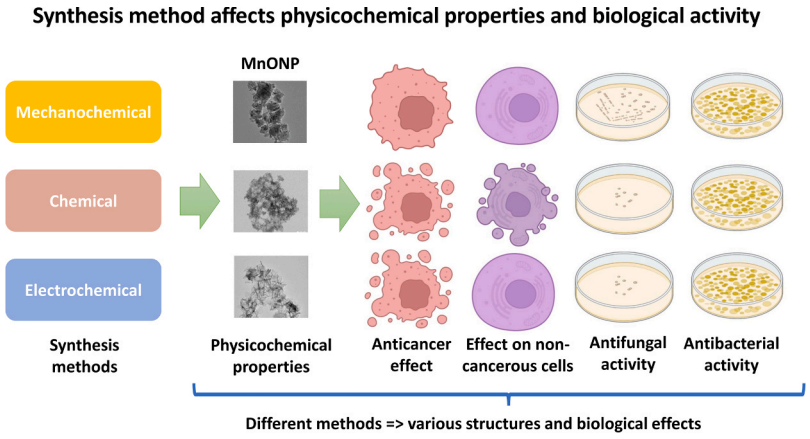

ARTICLE INFO

Keywords:
MnOx NPs

ABSTRACT

Manganese oxide containing nanoparticles (MnOx NPs) have emerged as promising antimicrobial and anticancer agents due to their unique properties. However, the different initial materials and synthesis techniques often

Abbreviations: MnOx NPs, manganese oxide containing nanoparticles; MM, milled MnOx; EM, electrophoretically deposited MnOx; SM, stirred precipitated MnOx; CM, commercial manganese oxide; SEM, scanning electron microscopy; TEM, transmission electron microscopy; XRD, X-ray diffraction; DSC, differential scanning calorimetry; EDS, energy dispersive X-ray spectroscopy; DLS, dynamic light scattering; XPS, X-Ray Photoelectron Spectroscopy; MIC, minimal inhibitory concentration; SZMC, Szeged Microbiology Collection; IFM, Research Center for Pathogenic Fungi and Microbial Toxicoses, Chiba University; ANOVA, one-way analysis of variance.

* Correspondence to: Department of Biochemistry and Molecular Biology, University of Szeged, Közép fasor 52, Szeged H-6726, Hungary.
E-mail addresses: kiricsim@bio.u-szeged.hu, kiricsim@gmail.com (M. Kiricsi).

[1] These authors contributed equally.

https://doi.org/10.1016/j.colsurfa.2024.133528
Received 12 September 2023; Received in revised form 19 December 2023; Accepted 21 February 2024
Available online 23 February 2024

nanoparticle synthesis
antimicrobial activity
antifungal activity
selective cytotoxicity
nanotherapeutics

yield nanoparticles with highly different properties which limit their applications especially in the biomedical field. Thus, we aimed to explore the suitability of pyrolusite as a new and sustainable manganese mineral source for MnOx production. Moreover, we examined the effect of various synthesis methods on the physicochemical characteristics and biological activity of MnOx NPs to explore their therapeutic utilization potential against microbes and in cancer treatment. We produced MnOx NPs from a naturally occurring mineral via mechanochemical, chemical, and electrochemical processes, characterized them thoroughly, and assessed their cytotoxicity against bacteria, fungi, and human cancerous and non-cancerous cells. We verified that the synthesis method utilized to obtain MnOx NPs impacted significantly nanoparticle properties leading to distinct structural, morphological, and biological characteristics. Although none of the particles was effective against the tested bacterial strains, electrochemically produced NPs demonstrated significant antifungal activity. These nanoparticles were also the most potent anticancer agents, exhibiting cancer-selective toxicity attributed to apoptosis induction rather than altered cell proliferation or direct necrotic effects. These results are relevant for the development of effective and safe nanotherapeutics and highlight the potential of MnOx nanoparticles - obtained through carefully selected initial mineral source and adequate synthetic approach - in antimicrobial and anticancer therapy.

1. Introduction

Due to the extensive utilization of nanomaterials in various fields of industry, technology, as well as medicine, the worldwide demand for nanoparticles is rapidly increasing [1]. For instance, metal-based nanoparticles are frequently employed in electronics, optics, in domestic items and in a wide range of medical applications, that led to an enormous rise in metal nanomaterial production [2,3]. Since initial precursor sources may vary and also the synthesis methods – i.e. chemical reduction, electrochemical processes, photochemical reactions, thermal/radiation-assisted methods, mechanical milling – are constantly evolving, these have to be adapted and adjusted to each other in order to provide nanomaterials with the required properties in the most efficient and cost-effective way. Therefore, optimalization of the source material and the production technology followed by the inspection of the nanomaterials' effects is a perpetual and relentless endeavor in nanomaterial science. The major challenges include insufficient stabilization, polydispersity, undesired chemical entities, which can severely limit the (biomedical) application possibilities of the produced nanomaterials.

In recent years, numerous nanoparticle-based therapies and imaging technologies have emerged for the purpose of elucidating biological processes and monitor disease conditions [4,5], and to deliver or act as therapeutic agents at targeted cells [6]. Inorganic materials like metal and metal oxide nanoparticles, especially silver, gold and iron-oxide, have been massively tested for biomedical and healthcare applications, among them tissue engineering, immune engineering, drug delivery, disease diagnosis, as a specific treatment agent or a biosensor [4–8]. It turns out that nanomaterials can be utilized very efficiently in antimicrobial and anti-cancer treatment modalities in particularly challenging cases such as multidrug resistance or infected patients suffering from multiple complications (immunocompromised, elderly individuals, premature newborns). Among several metal-based nanomaterials, manganese oxide containing nanoparticles (MnOx) were shown to exhibit impressive antimicrobial activity against various pathogenic species, such as *Escherichia coli*, *Klebsiella pneumoniae* and *Pseudomonas aeruginosa* and it was revealed that the toxicity of these nanoparticles against *E. coli* is primarily related to membrane damage but not to oxidative stress-induced lipid peroxidation [9–11]. It was also recently published that manganese can be exploited also for cancer immunotherapy, chemo-dynamic therapy, and magnetic resonance imaging, thus manganese oxide nanoparticles are now regarded as a novel platform for cancer theranostics [12,13]. Due to their pH-responsive degradation and versatile catalytic activities manganese- and manganese-oxide-based nanoparticles (MnOx NPs) in various oxidation states interact both with cells and their environment in a unique manner, furthermore, their magnetic susceptibility enables them to be easily guided to specific locations in the body (preferentially to the tumor site) using magnetic fields and enhance significantly the T1-magnetic resonance imaging contrast for tumor-specific imaging. In general, these particles seem to be well tolerated by the body and do not cause significant toxic effects in most tissues as they transform to harmless water-soluble Mn^{2+} ions which are then either quickly excreted by the kidneys (thus relieve the long-term toxicity concerns upon *in vivo* applications). Nevertheless, MnOx NPs show potent dose-dependent cytotoxic activity against human lung cancer cells, and reduce significantly the viability of human prostate cancer cells *in vitro* [14,15]. Moreover, MnO_2 nanostructures are capable of modulating the tumor microenvironment by triggering the decomposition of hydrogen peroxide into water and oxygen, forming a Mn-based tumor microenvironment-responsive multifunctional nanoplatform [16]. Based on these observations MnOx nanoparticles might hold enormous potential in clinical microbiology and in oncology to overcome the previously detailed limitations and challenges of diagnosis and treatment.

While several methods have been successfully employed to generate MnOx NPs, utilizing a broadly accessible, and naturally occurring mineral for nanomaterial synthesis offers several benefits especially in terms of production costs. Fortunately, manganese stands out as the second most abundant transition metal in the Earth's crust, as these manganese minerals participate in geochemical redox reaction processes and have a crucial function in the biological respiration process and the nutritional circle. Due to the variety of oxidation states and compositions, there are about 190 manganese minerals with a Mn content 25% or greater. Among these, about 30 encompass predominantly oxides, hydroxides, and carbonates that dominate the phases in commercial ores. Hungary has several manganese deposits, most of these have ores with a sedimentary origin. The ores from Úrkút, Hungary consist mainly of manganese carbonate minerals and a minor amount of pyrolusite—a black, amorphous mineral with a granular or columnar structure, displaying a metallic luster, and exhibiting a black streak. Moreover, our previous findings indicate that this indigenous mineral, the pyrolusite, holds enormous potential, since it can act as a direct precursor for synthesizing supercapacitor electrodes.

Drawing upon these facts, our objective was to delineate whether the mineral pyrolusite could be utilized for MnOx nanoparticle production, moreover, which synthesis approach would be the best suited process to exploit this source material for cost-effective nanomaterial manufacturing. Another aspect of our investigation, and is one of the major questions for production, whether and how a naturally occurring mineral that has only undergone simple processing methods, can be contemplated for certain applications involving biological entities. This can be considered as a relevant novelty component of this work. Along these lines, in the present research work mechanochemical, chemical, and electrochemical synthesis processes were applied and the produced MnOx nanoparticles were characterized for several physicochemical properties, among these size, shape, and crystalline structure. To examine the influence of the synthesis mode on biological activity and

on future medical applicability, the cytotoxicity of the various MnOx nanoparticles was examined on Gram-positive and Gram-negative bacteria, fungi and also on human cancerous and non-cancerous cells. Our results revealed that the applied synthesis methods used to produce nanoparticles from this naturally occurring mineral in fact had a significant impact on nanoparticle properties and on their biological performance. Importantly, MnOx nanoparticles produced by electrophoretic deposition exhibited the most prominent activity against yeast and various cancer cells, therefore, the most optimal synthesis approach that yields nanoparticles with the most outstanding potential regarding this nanomedicinal application can be selected.

2. Materials and methods

2.1. Materials

A brown-black manganese mineral sample of Úrkút, Hungary was received from the Institute of Geology, University of Szeged.

2.2. Synthesis of manganese oxides

2.2.1. Preparation of milled manganese mineral (MM)

The mechanically ground mineral was milled using a planetary ball mill, equipped with 20 steel balls, each weighing 4 g, in a 200 mL Ni/Fe/Cr milling bowl with the diameter of 50 mm. The direction of the milling was reversed every fifteen minutes, and the milling speed was 450 rpm. After two hours of dry milling, approximately 5 mL of ultrapure water was added to the milling bowl, and the milling continued for additional two hours at the same milling speed. After the second milling step, the sample was washed three times with water and three times with ethanol solution respectively. The filtered substance was freeze-dried overnight and stored in a dry sample tube.

2.2.2. Dissolution of milled mineral for the subsequent synthesis approaches

The initial steps involved dissolving 0.03 g of MnOx in 20 mL of oxalic acid (0.1 M). Later, the dissolved solution was separated by a membrane of 0.45 μm pore size from the undissolved residues, such as silica, from the mineral composite. For each subsequent sample synthesis, 20 mL of manganese oxalate solution was used.

2.2.3. Electrophoretically deposited MnOx (EM)

For the electrophoretic deposition, 20 mL (0.1 M) of NaOH was added to the filtered manganese oxalate solution (20 mL). Then in a cell containing two carbon paper electrodes as anode and cathode, 5 Volt DC was applied by a Keithley 2280S-60–3 power supply to the mixture. After the application of the voltage, manganese hydroxide began to deposit on the surface of the electrode and it continued for two hours. Then the particles were collected, centrifuged at 4000 rpm for ten minutes to separate them from the solution, and washed three times with distilled water. As a final step, the EM-labelled samples were freeze-dried overnight and stored in a dry sample tube. Manganese hydroxide rapidly transforms to oxide by exposure to air [17].

2.2.4. Stirred precipitated MnOx (SM)

In parallel experiments, 40 mL of 0.1 M NaOH was added dropwise to 20 mL of filtered manganese oxalate solution. Due to changes in the pH of the solution, manganese hydroxide formed. The sample was stirred for 2 hours until manganese hydroxide formation was complete. The particles were then separated from the solution by centrifugation at 4000 rpm for ten minutes and washed three times with distilled water. The sample, which was labelled SM, was dried overnight by freeze-drying method and stored in a dry sample tube.

2.2.5. Commercial manganese oxide (CM)

Chemical grade (Molar Chemicals) manganese dioxide was used without further purification.

2.3. Characterization of the MnOx samples

In order to determine the crystal structure of the various manganese oxide samples, a Rigaku Miniflex II powder X-ray diffractometer equipped with a Cu Ka radiation source (l = 0.15418 nm) and running at 30 kV and 15 mA at room temperature and scanning at a rate of 1 degree per minute in the 10–80° 2θ range was used. To analyze the morphology of the obtained nanomaterials a FEI TECNAI G2 20 X-TWIN transmission electron microscope at 200 kV accelerating voltage and a Hitachi S-4700 Type II instrument scanning electron microscope at 30 kV accelerating voltage was applied. The elemental composition of the samples was analyzed by energy dispersive X-ray spectroscopy (Röntec Quantax^2 EDS). Samples were drop-casted from alcoholic suspension onto silicon wafers and measured at 20 kV accelerating voltage without any additional coating. The thermodynamic properties of the nanomaterials were determined by differential scanning calorimetric (DSC) analysis utilizing Q20 (TA Instruments) at RT – 600 °C with a constant airflow and heating–cooling rate of 5 °C min^{-1}. A SENTERRA II Raman microscope (Bruker Optics, Inc.) was used to acquire the Raman spectra at 532 nm with a 1 s integration time (with three repetitions) at a resolution of 4 cm^{-1} and an interferometer resolution of 0.5 cm^{-1}. The electrophoretic mobilities of manganese oxide particles in water-based and RPMI cell culture medium-based dispersions were examined by Nano ZS (Malvern) dynamic light scattering (DLS) apparatus with a 4 mW He-Ne laser source (λ= 633 nm) operating in backscattering mode and disposable zeta cells, respectively. To explore the exact oxidation states, X-ray photoelectron spectroscopy (XPS) measurements were performed. For this, samples were pressed onto double-sided carbon tapes attached to stainless steel sample holders. A Specs XPS instrument equipped with an XR50 dual anode X-ray source and a Phoibos 150 hemispherical analyzer was used for the measurements. The Al Kα X-ray source was operated with 150 W (14 kV) power. Survey spectra were collected with 40 eV pass energy and 1 eV step size. High-resolution spectra were collected with 20 eV pass energy and 0.1 eV step size. Collected high-resolution spectra were C 1 s, O 1 s, and Mn 2p. For data evaluation the CasaXPS software version 2.3.25PR1.0 was used [18]. All high-resolution spectra were background corrected with a Shirley background and all peaks were fit with a Gauss-Lorentzian product function where the Lorentzian contribution is 30%.

2.4. Antimicrobial activity of MnOx particles

2.4.1. Determination of minimal inhibitory concentration (MIC)

Growth inhibition of the MnOx NPs was tested in 96-well microtiter plates on *Escherichia coli* SZMC 0582 (SZMC: Szeged Microbiology Collection), *Bacillus megaterium* SZMC 6031 and *Cryptococcus neoformans* IFM 5844 (IFM: Research Center for Pathogenic Fungi and Microbial Toxicoses, Chiba University) strains. The minimal inhibitory concentration (MIC) was determined with the microdilution method by adding 50 μL serially two-fold-diluted nanoparticle solution to 50 μL of cell suspension (8×10^4 cell/mL) in RPMI 1640 medium (Biosera, Nuaille, France). The applied concentration range for each nanoparticle was 5–0.019 mg/mL, the dilution was made in RPMI 1640 medium. After 48 hours (*E. coli, B. megaterium*) or 72 hours (*C. neoformans*) of incubation at 30 °C, the optical density of the cultures was measured at 620 nm in SPECTROstar Nano plate reader (BMG LabTech, Offenburg, Germany). Cell suspension supplemented with 50 μl RPMI 1640 was used as growth control. Minimal inhibitory concentration was defined as growth inhibition ≥ 90% compared to 100% growth of the untreated control. The experiments were carried out in three biological repeats always in triplicates.

2.4.2. Cell viability test

For cell viability test, 50 μL samples were taken from the cultures at the end of the incubation period, and the samples were diluted to 10- and 100-fold in sterile distilled water. From each dilution (10^{-1} and

10^{-2}) as well as from the undiluted sample (dilution 10^{0}) 5 μL were placed on solid medium and the growth of the strains was detected after 48-hour incubation at 30 °C. YPD medium (1% peptone, 1% dextrose, 0.5% yeast extract and 2% agar) was used for cultivation of *C. neoformans*. *E. coli* and *B. megaterium* were propagated on meat extract-peptone medium (1% dextrose, 0.5% meat extract, 0.5% peptone, 0.1% yeast extract and 2% agar).

2.5. Anti-cancer activity of MnOx particles

2.5.1. Cell culturing

MCF-7 human breast adenocarcinoma, DU-145 human prostate cancer, and MRC-5 human fibroblast cell lines were purchased from ATCC. MCF-7 and DU-145 cells were maintained in RPMI-1640 (Biosera, Nuaille, France), MRC-5 cells were maintained in EMEM medium (Biosera, Nuaille, France) complemented with 10% FBS, 2 mM L-glutamine, 0.01% streptomycin and 0.005% penicillin and cultured under standard conditions in a 37 °C incubator containing 5% CO_2 in 95% humidity.

2.5.2. MTT cytotoxicity assay

To investigate the cytotoxicity of the manganese oxide containing samples (MM, EM, SM, CM), first the viability of various cancer cells and of non-cancerous fibroblasts following treatments were detected by MTT assay. For this, 10,000 cells/well (MCF-7, DU-145 human adenocarcinoma or MRC-5 human fibroblasts) were seeded into 96-well plates and left to grow. The next day cells were exposed to increasing concentrations of MM, EM, SM, CM nanoparticles (0; 18.75; 37.5; 75; 150; 300; 600 μg/mL). After 24-hour incubation, the nanoparticle-containing media were removed, cells were washed with PBS and then incubated with 0.5 mg/mL MTT (Sigma-Aldrich, St Louis, Missouri, USA) for 1 h in a 37 °C incubator. The formazan crystals were solubilized in DMSO (Molar Chemicals, Halásztelek, Hungary), the absorbance of the samples was determined at 570 nm using a Synergy HTX plate reader (BioTek, Winooski, Vermont, USA). The viability measurements were repeated three times using 3 independent biological replicates.

2.5.3. BrdU proliferation assay

The anti-proliferative effect of MnOx nanoparticles (MM, EM) on cancerous cells was assessed by BrdU assay. To measure the rate of cell proliferation, 5000 MCF-7 or DU-145 cells were seeded into 96-well plates. On the following day, the cells were treated with MnOx nanoparticles at 4.5 μg/mL concentration for 48 hours. After the treatments, BrdU solution (Roche, Basel, Switzerland) was added to the samples (1:5000 dilution) and the samples were incubated for 3 hours. Then cells were fixed, washed and the anti-BrdU antibodies were added to the wells according to the manufacturer's instructions. After 90-minute incubation with the antibodies, 100–100 μL substrate was added to the samples and the absorbance was measured at 370 nm with Synergy HTX plate reader (BioTek, Winooski, Vermont, USA).

2.5.4. LDH assay

The LDH assay was performed on MCF-7 as well as on DU-145 cells after MM, EM sample treatments. For this, 15,000 cells were seeded into 96-well plates and left to grow. On the next day, cells were treated with 10 or 40 μg/mL MM or EM nanoparticles. Following a 24-hour incubation, the supernatant of each well was replaced to a new plate and 100 μL LDH working solution (Dojindo Molecular Technologies, Rockville, Maryland, USA) was added to the samples according to the manufacturer's instruction. After 30 min incubation the absorbance of the samples was measured at 490 nm with Synergy HTX plate reader (BioTek, Winooski, Vermont, USA).

2.5.5. Analysis of apoptosis induction

The expression of several apoptosis marker genes was determined by reverse transcription followed by real-time qPCR. For this, MCF-7 and DU-145 adenocarcinoma cells were seeded in 60 mm tissue culture dishes (6×10^{5} cells/dish) and left to grow overnight. Then cells were treated with 40 μg/mL of either MM, EM MnOx nanoparticles. After a 24-hour treatment, cells were collected and total RNA was isolated using RNeasy® Mini Kit (QIAGEN, Hilden, Germany) by following the manufacturer's instructions. 2 μg RNA was reverse transcribed (TaqMan® Reverse Transcription kit, Applied Biosystems, Foster City, CA, USA) in 50 μL total volume. PCR reactions were performed on PicoReal™ Real-time PCR (Thermo Scientific, Waltham, MA, USA) using SYBRGreen qPCR Master Mix (Thermo Scientific, Waltham, MA, USA) with an input of 2 μL cDNA. Each primer (Table 1) was used at 200 nM concentration. Thermal cycling was performed as follows: 10 min at 95 °C, then 40 cycles of 95 °C for 15 sec and 60 °C for 1 min. Relative transcript levels were determined by the ΔΔCt analysis using GAPDH as reference gene. Experiments were repeated three times with three biological replicates.

2.5.6. Statistical Analysis

Data are presented as the mean ± standard deviation (SD). GraphPad prism software was used to evaluate statistical differences by one-way analysis of variance (ANOVA) followed by Fisher's LSD tests. Criterion for statistical significance was set at $p < 0.05$. The representative significance values as per Fisher's LSD test are *, $P<0.03$ **, $P<0.002$ ***, $P<0.0002$ ****, $P<0.0001$.

3. Results and discussion

3.1. Structural differences of MnOx nanoparticles obtained by various synthesis methods

Following syntheses, the obtained samples were characterized by multiple techniques, among them X-ray diffraction spectroscopy to reveal the crystal structure of the materials. Fig. 1**A** demonstrates the X-ray diffraction (XRD) pattern of the samples. The initial sample (MM) and the commercial manganese dioxide (CM) were confirmed to be manganese dioxide through XRD analysis. Strong reflections were observed at 28°, 37° and 57° that can be linked to the reported data of beta manganese dioxide [19]. In the case of EM and SM samples, reflection peaks are weak and difficult to distinguish due to the highly amorphous nature and consequently shorter range order of the structure. However, the low intensity peaks at 18° and 36° indicated that both samples contained a detectable amount of Mn_3O_4 phase [20]. Raman spectra were also collected from the 4 different materials (displayed in Fig. 1**B**). Raman shifts at 662 cm^{-1} and 538 cm^{-1} were observed for CM samples, which correspond to the MnO_2 reference data [21]. The two merged Raman shifts at 580 cm^{-1} and 640 cm^{-1} indicate that MM, SM and EM samples contain Mn_3O_4 [22]. Nevertheless, Buciuman et al. suggested that the appearance of the Mn_3O_4 in a mostly MnO_2 sample, like our MM, can be linked to the formation of the Mn_3O_4 phase during spectrum acquisition, because of the local heating of the sample [23].

The chemical compositions of the samples detected by energy dispersive X-ray spectroscopy (EDS) are displayed in Table S1. These data revealed that MM and EM samples have comparable levels of manganese (Mn) and iron (Fe), 43.8–42.2 wt% and 6.1–7.1 wt%, respectively. However, the SM sample contains more iron (13.6 wt%) than the other three samples. Manganese oxides have distinct

Table 1
Primers and their sequences used for RT-qPCR analysis.

Target	FWD primer	REV primer
GAPDH	GAGTCAACGGATTTGGTCGT	TGGAAGATGGTGATGGGATT
bax	TGCTTCAGGGTTTCATCCAG	GGCGGCAATCATCCTCTG
p53	CCCTTCCCAGAAAACCTACC	CTCCGTCATGTGCTGTGACT
p21	CAGCAGAGGAAGACCATGTG	GGCGTTTGGAGTGGTAGAAA
survivin	AGAACTGGCCCTTCTTGGAGG	CTTTTTATCTTCCTCTATGGGGTC
caspase-3	ACATGGCGTGTCATAAAATACC	CACAAAGCGACTGGATGAAC

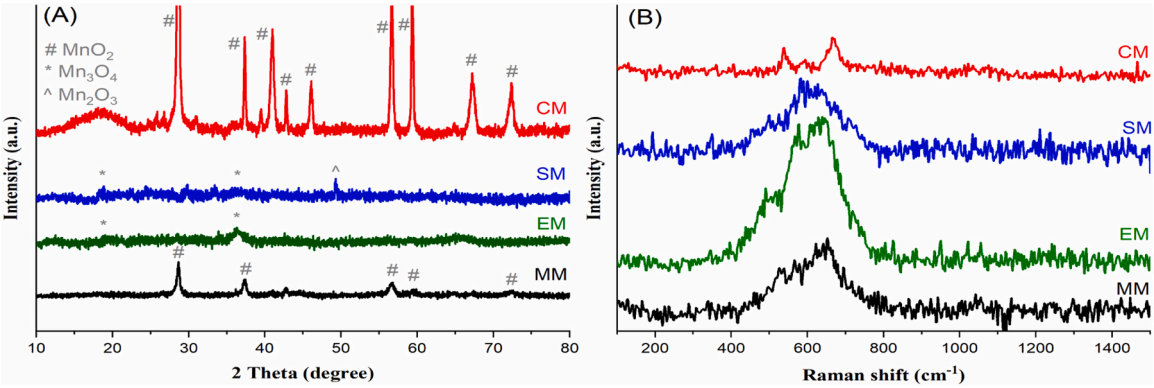

Fig. 1. X-ray diffraction patterns (A) and Raman spectra (B) of MM, EM, SM and commercial (CM) samples.

morphologies and particle sizes, and as the initial material was a naturally originated mineral sample, the resulted nanoparticles could contain Fe impurities even in relatively larger quantities. However, we have to note that Fe can either increase the biological activity of the material or alter the Mn oxidation state ratio [24]. It was demonstrated that the oxidation rate of Mn^{2+} increases but the crystallinity of manganese oxides significantly decreases in the presence of Fe^{2+}. It was proven that mixed iron-manganese NPs have cytotoxic effect on human breast cancer cell line via promoting tumor-responsive ferroptosis [25].

Differential scanning calorimetric analysis (Fig. S1) shows the transition in the samples as a function of time and temperature. These data indicate that particles in sample MM have an amorphous-like structure, and upon scanning two small exothermic peaks appear due to crystallization. On the other hand, no crystallization peak was observed in case of CM sample, where the only strong endothermic peak was seen at 500 °C due to phase changes of MnO_2 to Mn_2O_3 [26]. Nevertheless, thermodynamic properties and thermal analysis confirmed that both samples are of MnO_2. The thermal decomposition steps of samples SM and EM were similar. Exothermic crystallization peaks were observed in both samples around 250–350 °C, however, no endothermic (melting) peak appeared, in contrast to MnO_2 samples (MM and CM).

The particle size and shape of the initial milled manganese dioxide MM were determined by SEM and TEM image analysis (Fig. 2). These indicate a particle size of about 200–500 nm, and MM particles appeared plate-like and amorphous. In the case of the EM sample, TEM and SEM images revealed flower-like tiny flakes with an average size of 50–100 nm. The SM sample contained sheet-like particles, with a size of about 100–500 nm. Finally, the CM sample was made of 500 nm to a few micrometer-sized rod-like particles (Fig. 2).

The x-ray photoelectron (XPS) spectra of the four materials (MM (a), SM (b), EM (c) and CM (d) are illustrated in Fig. S2. The oxidation states of manganese were distinguished with a fitting approach, where multiplet splitting was taken into consideration [27]. The peak models for MnO, Mn_2O_3, and MnO_2 as presented in the work of M. Biesinger *et al.* were compared against the Mn 2p 3/2 signal of the examined samples, allowing ±0.2 eV shift for the first component of a given oxidation state and leaving the rest of the parameters restricted according to the literature. After achieving the best fit, the ratio of different oxidation states was calculated from the ratio of the area of the multiplet component peaks. As it can be seen, manganese in all 4 samples is in the state of Mn^{4+} and Mn^{3+} (Table S2). Although the ratio of MnO_2 and Mn_2O_3 varies, it can be stated that the mineral-derived samples contain more Mn_2O_3 phase compared to the commercial manganese oxide, which can cause a modified biological behavior (Table S2). Among three common manganese valences within MnOx, Mn^{2+} ions show the best stability due to half-full outer 3d electrons compared with Mn^{3+} ions and Mn^{4+} ions. Therefore, Mn^{3+} ions and Mn^{4+} ions are prone to oxidation, can react with intracellular reducing substances, like GSH. This interaction between oxidizing MnOx and cells leads to intracellular GSH depletion, which further affects a series of complicated biochemical reactions including nanomaterials and cells. Thus, compared to Mn^{2+} ions, it has been proven that higher-valenced MnOx at the same manganese content showed higher cancer cell killing due to GSH depletion [28].

As a final step of nanomaterial characterization, DLS measurements were carried out to assess the surface charges and thereby the colloidal stability of the particles in two different media, namely in distilled water as well as in RPMI cell culture medium (Fig. 3**)**. The zeta potential value of the samples differs more clearly when these are suspended in water than in culturing media (RPMI). In water suspension, EM and CM samples had similar negative potentials of about −16 to −25 mV in the entire concentration range tested (50–600 μg/mL). The MM sample had

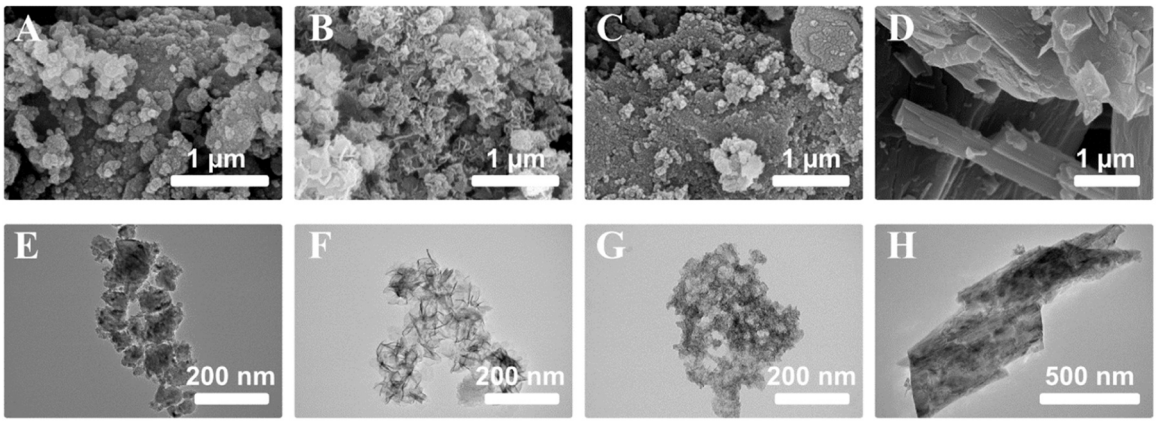

Fig. 2. Scanning electron microscopic (A-MM, B-EM, C-SM, D-CM) and transmission electron microscopic images of the samples (E-MM, F-EM, G-SM, H-CM).

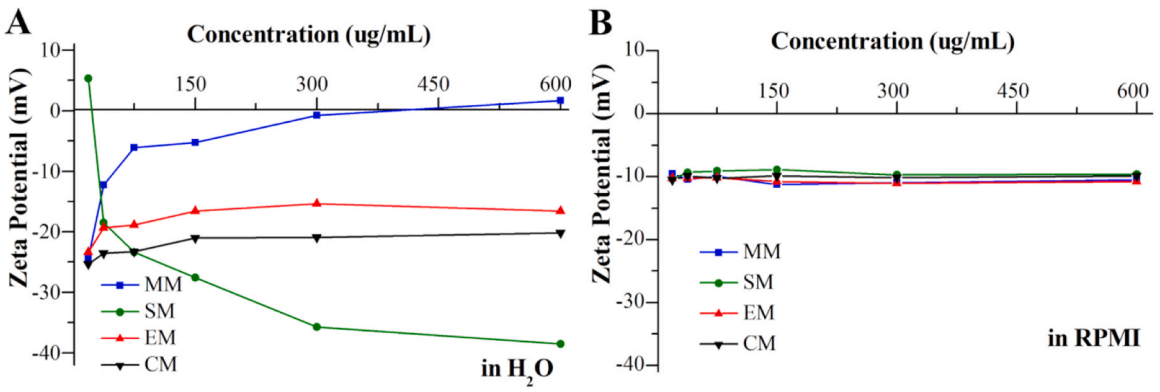

Fig. 3. Zeta potential of the samples in water (A), and in RPMI medium (B).

a negative zeta potential (−24 mV) at lower concentrations (below 18.75 μg/mL), however, the zeta potential resulted to be much higher as the nanoparticle concentration increased, in fact, at 600 μg/mL concentration it was 1 mV. On the contrary, SM particles exhibited more negative surface charges at 300–600 μg/mL than at lower concentrations. The zeta potential reached the value of −40 mV at the highest applied nanoparticle concentration, which potential was 2 times higher than those of EM and CM samples. In RPMI media, the zeta potential value of the samples was the same, around −10 mV, and it did not change within the entire concentration range tested (Fig. 3).

3.2. *Biological activity of MnOx nanoparticles synthetized by different methods*

3.2.1. *Antimicrobial activity*

The antimicrobial activity of MnOx nanoparticles (MM, EM, SM, CM)

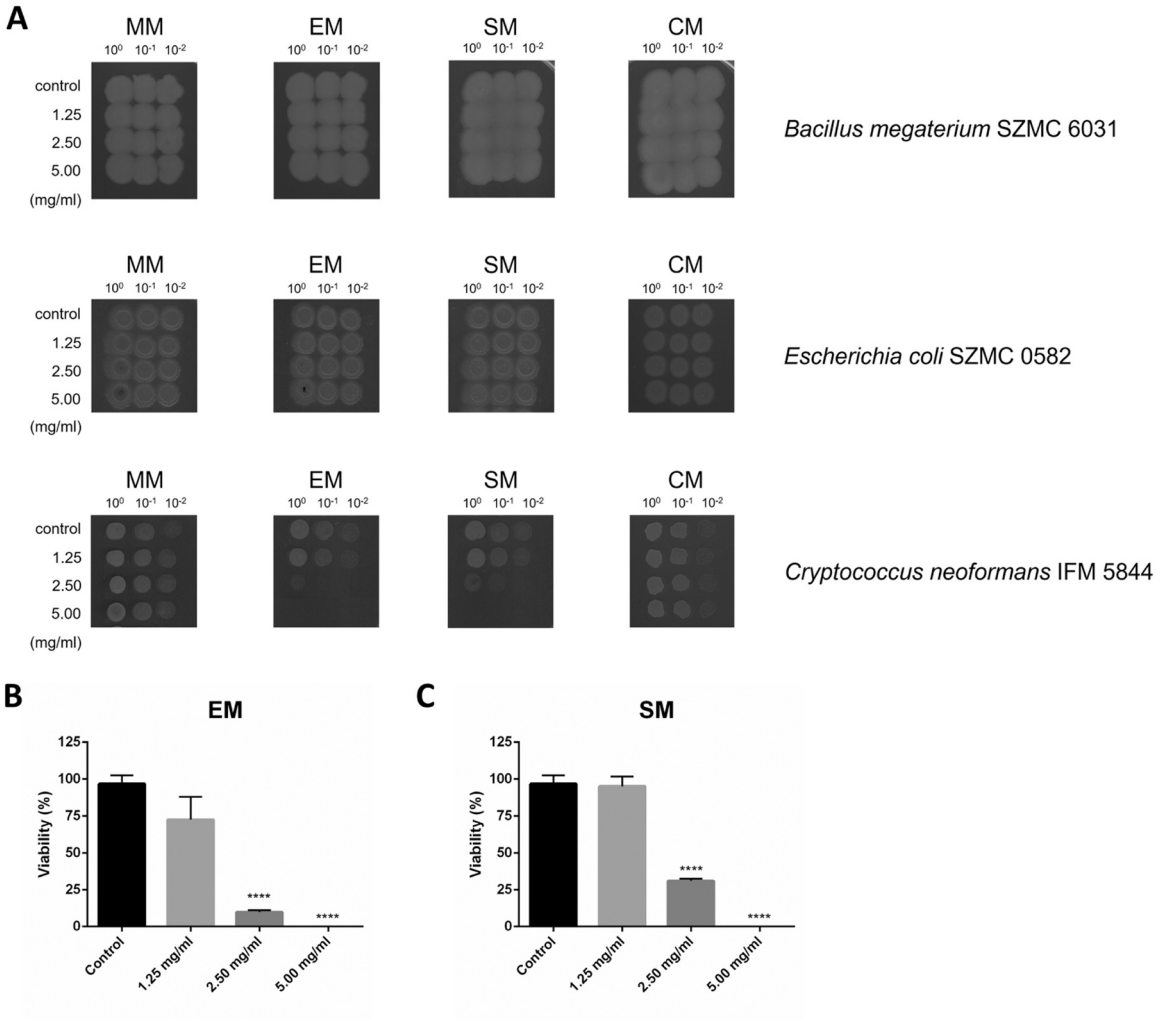

Fig. 4. Antimicrobial activity of MM, EM, SM, CM nanoparticles against bacteria (*E. coli* and *B. megaterium*) and yeast cells (*C. neoformans*) (A) and quantitative assessment of *C. neoformans* viability upon treatments with EM (B) and SM nanoparticles (C). 10^0, 10^{-1} and 10^{-2} represent the scale of the dilution.

was tested against bacteria (*E. coli* and *B. megaterium*) and yeast cells (*C. neoformans*). None of the four nanoparticles were toxic for *E. coli* and *B. megaterium* even at the highest applied concentration (5 mg/mL). Against *C. neoformans*, neither MM nor CM was effective, however EM and SM particles exhibited a moderate to strong growth inhibitory activity. The minimal inhibitory concentration of EM and SM particles was established at 5 mg/mL, furthermore, EM decreased the number of viable cells with two, whereas SM with one orders of magnitude at 2.5 mg/mL concentration (Fig. 4).

3.2.2. Anticancer activity

Toxicity of MM, EM, SM and CM nanoparticles were assayed on MCF-7, DU-145 human cancer cell lines and on MRC-5 human fibroblast cells (Fig. 5).

No toxic effect of MM and CM nanoparticles was observed on the applied cells. On the other hand, SM nanoparticles decreased the cell viability of the cancerous DU-145 and the non-cancerous MRC-5 fibroblast cells, however, were non-effective on the cancerous MCF-7 cells. The best performance was shown by the EM-labeled nanoparticles, since EM was highly toxic already at low concentrations to MCF-7 as well as DU-145 cancer cells, and did not decrease strongly the viability of MRC-5 fibroblast cells. Based on the above, for further, more detailed cell and molecular biology examinations, EM nanoparticles were selected. We included MM nanoparticles also into the following experiments as a control, since they did not induce any toxic effect on any cell line tested.

The MTT assays were repeated and based on the viability data on MCF-7, DU-145, MRC-5 cells upon MM and EM nanomaterial treatments, the IC_{50} values of these nanoparticles on each cell line were obtained. The IC_{50} values calculated according to the dose-response curves are shown in Table 2. These values support the cancer cell-selective feature of EM nanoparticles, since each IC_{50} value determined on cancerous cell lines is of one magnitude smaller than on non-cancerous MRC-5 fibroblasts.

Table 2
IC_{50} values of selected nanoparticles (MM and EM) on DU-145 prostate and MCF-7 breast cancer cells as well as on non-cancerous MRC-5 fibroblasts based on MTT cell viability assays. Cell density was 10^4 cells/well, treatment time was 24 h.

Cell lines	IC_{50} values for MM	IC_{50} values for EM
DU-145	> 600 μg/mL	31.58 μg/mL
MCF-7	> 600 μg/mL	4.05 μg/mL
MRC-5	> 600 μg/mL	556.2 μg/mL

To investigate the reason behind the viability decrease of MCF-7 and DU-145 cancer cells upon EM nanoparticle exposures, we treated these cells either with EM or as a control with MM nanoparticles, then BrdU proliferation assay and LDH release assay were performed, furthermore, the expression of several apoptosis marker genes were examined. For the proliferation assay, subtoxic concentration of each nanoparticle was selected and both MCF-7 and DU-145 adenocarcinoma cells were incubated with the nanoparticles for a longer period of time (at 4.5 μg/mL, 48 h). According to our results neither MM nor EM NPs could affect the cell proliferation of cancerous MCF-7 or DU-145 cells, since in each case the BrdU incorporation was similar to that of the untreated control cells (see Fig. 6**A**). Therefore, we concluded that the previously observed cancer-selective toxicity of EM nanoparticles was not the result of attenuated cell proliferation.

Since cell proliferation was not affected by EM nanoparticles we examined necrosis and apoptosis as possible mechanisms behind nanoparticle-induced toxicity. For this, LDH release assay was first performed on MM or EM NP-exposed cancer cells. Results indicate that nanoparticle treatment did not induce necrosis in these cancer cells,

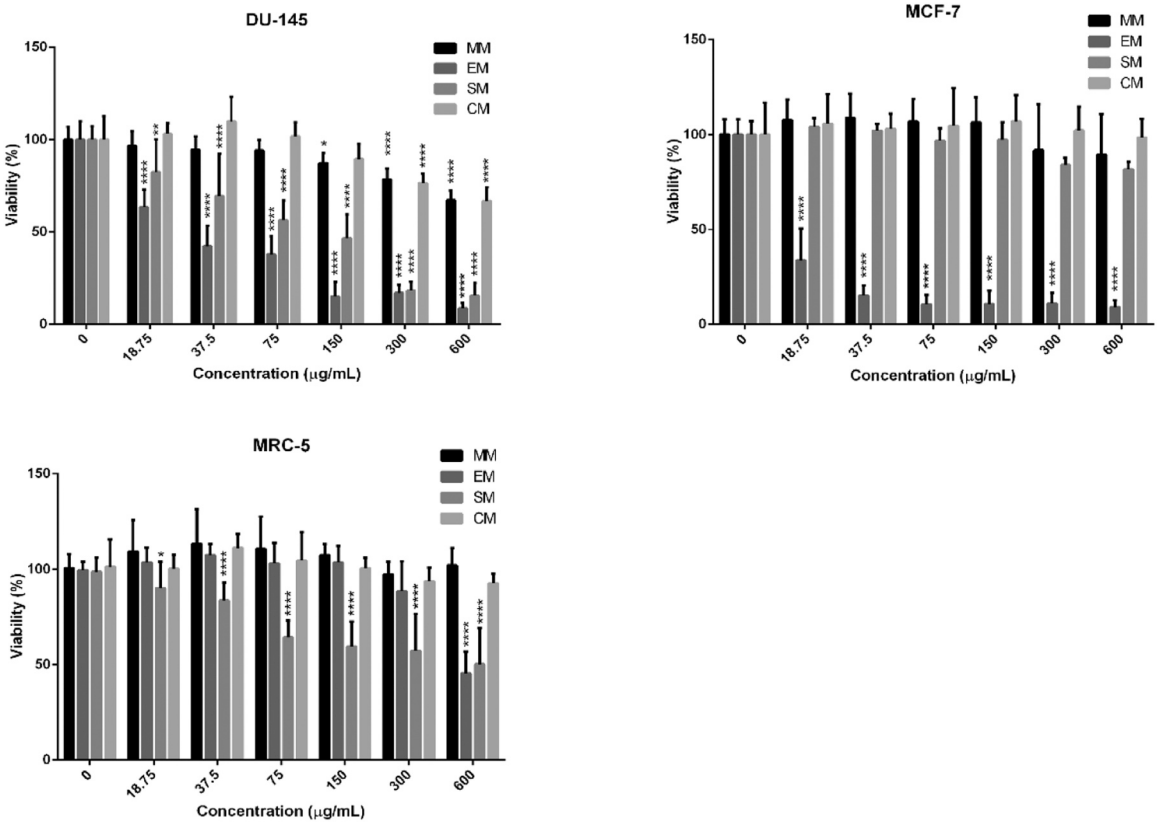

Fig. 5. Viability of DU-145 and MCF-7 adenocarcinoma cells as well as of MRC-5 human non-cancerous fibroblasts following 24-hour exposures to MM, EM, SM, CM-labeled nanoparticles applied in various concentrations, assessed by MTT cell viability assay. Bar graphs represent mean ± SD values. Fisher's LSD test, *: $P < 0.05$, **: $P < 0.01$, ****:$P < 0.0001$.

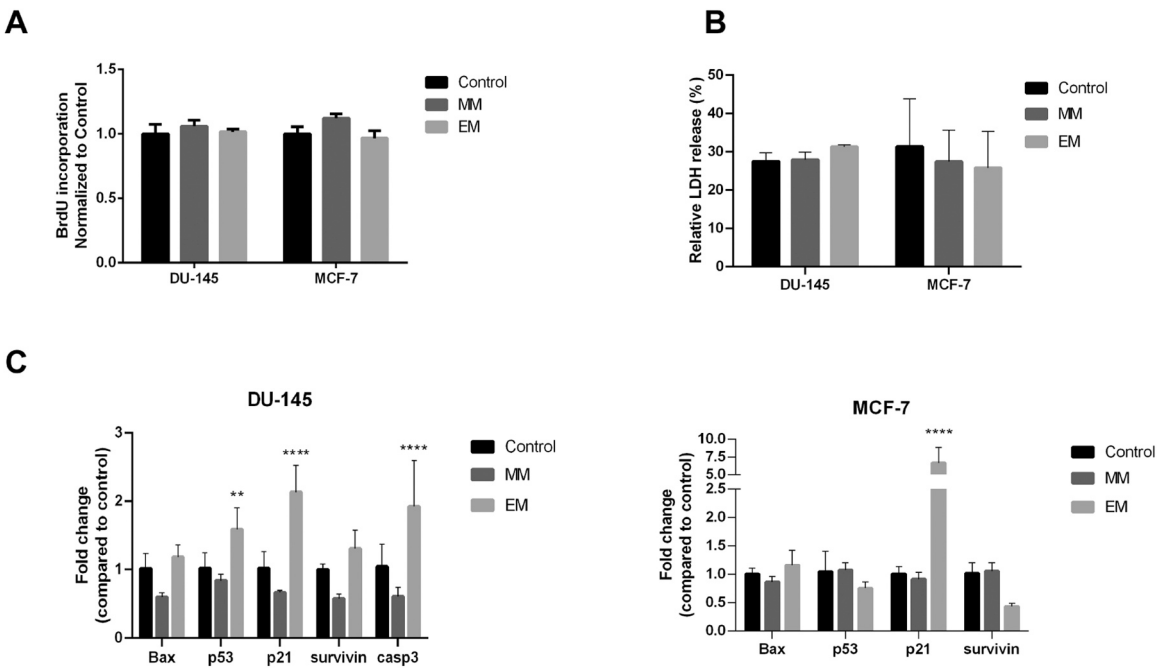

Fig. 6. Cell proliferation, LDH release and apoptosis induction in DU-145 and MCF-7 cancer cells following MnOx NP treatment. Proliferation of untreated and MnOx NP-treated cancer cells examined by BrdU incorporation assays. Values are expressed as mean ± SD and compared to untreated control groups (**A**). The effect of MM and EM NPs on the LDH release of DU-145 and MCF-7 adenocarcinoma cells. Values were normalized to background and were expressed as percentage relative to total cellular LDH activity. Bar graphs represent mean ± SD values. Fisher's LSD test. (**B**) Apoptosis induction by MM and EM nanoparticles was verified by determining the relative mRNA levels of apoptotic markers Bax, p53, p21, survivin, Casp-3, in DU-145, and Bax, p53, p21, survivin in MCF-7 cells. Fisher's LSD test, *: P<0.05, **: P<0.01, ***: P<0.001, ****: P<0.0001. (**C**).

since the LDH release was not elevated upon MnOx NP administration (Fig. 6**B**).

Apoptosis induction was examined by determining the expression levels of various apoptosis marker genes, such as *Bax, p53, p21, survivin* and *caspase-3* in untreated MCF-7 and DU-145 adenocarcinoma cells as well as in cancer cells exposed to MM or EM-labeled nanoparticles. Our results indicate that in fact, apoptosis was triggered by EM NPs in both types of cancer cells. In DU-145 prostate cancer cells the apoptosis induction by EM nanoparticles was verified by significantly increased p53, p21, and caspase-3 gene expression levels, in MCF-7 cells by 6-fold enhanced p21 levels. The mRNA level of caspase-3 in MCF-7 cells was not assayed as these cells are known to be caspase-3-negative. As expected, no apoptosis induction was verified in cancer cells treated with MM nanoparticles. These results support that EM NPs exert their cancer-selective toxicity by triggering apoptosis.

4. Discussions

The application of nanotechnology in modern medicine has expanded the range of treatment approaches, particularly in clinical microbiology and cancer therapy. The utilization of metallic nanoparticles to develop antimicrobial and anticancer agents has emerged as a promising alternative to traditional pharmaceuticals [29]. The basis of this notion lies within the exceptional and versatile properties of nanoparticles (e.g., large surface area to volume ratio, unique shape and size and reactivity, etc.) that allow them to interact with biological entities such as various microbes or cancerous cells at a nanoscale level, yielding outstanding therapeutic outcomes in forms of antimicrobial, anticancer or drug delivery agents. Among inorganic materials, manganese oxide-based nanomaterials were recently shown to exhibit exciting activities that should be exploited in clinical microbiology and oncology [30]. It was reported that manganese oxides, i.e. MnO_2 and Mn_3O_4, can be decomposed into water-soluble Mn^{2+} ions, which can be used for tumor recognition and diagnosis, and those manganese oxide species that are able to react with H_2O_2 can produce O_2 and compensate hypoxia in the tumor microenvironment [31].

As it has been highlighted above and suggested by previous papers, there is no doubt that the application of drugs containing MnOx NPs is of clinical importance particularly in the treatment of various infectious diseases and cancers. Albeit there is a wide variety of initial Mn sources and synthesis approaches available for the production of these NPs, several studies have shown that the nanoparticles synthesized via various methods demonstrate significant structural and morphological differences [32], [33]. In correlation with these physical and chemical properties the biological activity of the produced particles may differ significantly as well. Therefore, refining the protocols and methods for improving the effectiveness of NP production alone is not sufficient, we should also precisely know how these methodological factors affect the biological performance of the obtained nanoparticles to ensure safety upon their potential therapeutic utilizations, to pave the way for further nanomedicinal developments towards successful clinical applications, especially when the initial manganese source involved for the synthesis procedure has not yet been used for this purpose prior.

Accordingly, in this present work our primary goals were to explore the suitability of the broadly accessible, and naturally occurring mineral pyrolusite for MnOx NP synthesis, and reveal if it is possible to find an appropriate synthesis approach to efficiently capitalize it for nanomaterial production without involving complicated and expensive processing technologies. Finally, since the generated MnOx NPs were considered for ultimate biomedical application (following proper development), the extent and the mechanism of cytotoxicity exhibited by the various MnOx nanoparticles obtained using different methods was evaluated on of Gram-positive and Gram-negative bacteria, fungi and also on human cancerous and non-cancerous cells. The novelty component of the work does not imply *per se* the mechanochemical, chemical, and electrochemical synthesis processes that were applied to produce MnOx nanoparticles, which were then extensively characterized, but rather the implementation of pyrolusite and the identification

of the most suitable method to utilize this specific mineral as an input for NP production. Furthermore, this technical question was also regarded within the biological application context of the obtained nanoparticles, thereby creating a complex mineral source-synthesis technique-MnOx NP-biological impact-mechanism of biological toxicity axis for the presented work.

Thus, three different procedures were applied on the mineral sample and the nanoparticles were characterized using microscopic, spectroscopic and thermal techniques, comprising XRD, SEM, TEM and DLS. To assess the influence of the synthesis mode on biological activity and thus on medical applicability, the cytotoxicity of the obtained manganese oxide nanoparticles was evaluated and compared in various biological systems, including microbes and cancerous cells. Finally, the mechanism of cytotoxicity was delineated in case of the most effective and cancer cell selective nanomaterial.

Our results revealed that the synthesis method used to produce manganese oxide nanoparticles significantly affects their structural properties. XRD analysis and Raman spectra confirmed that the initial manganese oxide sample (MM) and commercial manganese oxide (CM) were manganese dioxide, while the EM and SM samples contained a significant amount of Mn_2O_3 and Mn_3O_4 phase. The chemical composition of the samples showed comparable levels of manganese and iron in MM and EM, with SM having a higher iron content. The residual or somewhat higher amounts of iron might be considered as a contaminant, however, in certain setups this feature can be advantageous. It is known that iron and various iron oxides have antimicrobial and antitumoral effects and could induce oxidative stress and cell death, furthermore, manganese can efficiently catalyze Fenton-like reactions, and thereby trigger the production of ROS at higher levels than iron. Moreover, it was also proven earlier that mixed iron manganese NPs exhibited antitumor activity via ferroptosis by the inactivation of phospholipid peroxidase glutathione peroxidase 4 (GPX4) due to highly efficient GSH depletion capability [28]. Based on these, the iron content of the material could as well be beneficial from the aspect of promoting the desired biological activity maybe in a synergistic manner. Thermal analysis revealed differences in crystallization behavior, with MM exhibiting small exothermic peaks and CM showing phase changes to Mn_2O_3. SEM and TEM images displayed different particle sizes and shapes, ranging from plate-like to rod-like particles. Zeta potential measurements indicated differences in surface charges, with EM and CM having similar negative potentials in water, while MM showed a higher potential at higher concentrations. SM particles exhibited more negative surface charges at higher concentrations. In RPMI media, the zeta potential values were similar for all samples.

These structural differences affected the biological activity of the nanoparticles and therefore these most certainly have serious consequences on the potential biomedical applications of manganese oxide nanoparticles as well. In this study we examined the possible antimicrobial activity of the differently synthesized MnOx nanoparticles using microdilution and cell viability methods, and also the impact of these nanomaterials on various cancerous and non-cancerous cells. Our results revealed that none of the as-prepared MnOx NPs was effective against the tested bacteria (*E. coli* and *B. megaterium*) even at the highest applied concentration, however, two out of the four manganese oxide samples - SM and particularly EM particles – proved to be efficient on the pathogenic yeast *C. neoformans*. The outstanding antifungal potential of SM and EM nanoparticles might be related to the fact that these samples contained a significant amount of Mn_2O_3 and Mn_3O_4 phase, which is probably more favorable over other manganese oxide forms at least upon encountering yeast cells [34]. The strongest activity against *C. neoformans* was exhibited by EM particles, which is possibly the result of some additional structural features, as these particles appear in flower-like tiny flakes and the average size of EM MnOx NPs is the smallest among the as-prepared nanomaterials of the study, since their size varied between 50 and 100 nm. Another aim of our study was to investigate the anticancer efficiency of these differently synthesized manganese oxide nanoparticles to be able to delineate which synthesis method yields the most suitable particles for a potential oncological application. Fairly early in the investigation it was clear that EM MnOx NPs accomplished the most effectively the elimination of various cancer cells, since they were killing breast as well as prostate adenocarcinoma cells in much lower concentrations than any of the other manganese samples examined in the study. SM particles were comparably toxic to DU-145 cells, however, MCF-7 breast adenocarcinoma cells remained viable upon SM treatments. Both EM and SM particles reduced somewhat the viability of non-cancerous fibroblasts, nevertheless, the more detailed examination of dose response and the determination of the IC_{50} values revealed that the IC_{50} values of EM nanoparticles on cancerous cell lines were one or two magnitude smaller than on non-cancerous MRC-5 fibroblasts. This is an important result as it proves that we can select adequate concentrations of EM particles which kill breast and prostate cancer cells but leave healthy cells intact, thus a cancer-selective activity can be achieved by applying EM nanoparticles. These observations were further supported by our XPS results, as these revealed that the mineral-derived samples contain more Mn_2O_3 phase compared to the commercial manganese oxide, which can possibly be linked to the increased biological activity of the former particles (Table S2). This is in line with what was presented in the work of Jiang *et al.*, in which the systematic evaluation of the catalytic and biological activities of three MnOx nanoparticles (MnO_2, Mn_2O_3, and Mn_3O_4 NPs) was established [34]. Cellular studies revealed concentration-dependent decreases in cell viability induced by all three MnOx NPs, with Mn_3O_4 exhibiting the highest cytotoxicity, followed by Mn_3O_2 and MnO_2 NPs.

To reveal the possible molecular mechanism induced by EM nanoparticles upon cancer cell elimination, we examined some cellular events such as cell proliferation, necrosis and apoptosis in MCF-7 and DU-145 cells following EM nanoparticle treatments. We found no signs of modulated cell proliferation and also no evidence of direct necrosis, assayed by BrdU incorporation as well as LDH release assays. However, we detected significant changes in the expression of numerous apoptotic marker genes triggered by EM-MnOx NPs both in MCF-7 as well as in DU-145 cancer cells. Especially EM nanoparticle-treated DU-145 prostate cancer cells were found to be apoptosis sensitive, as increased p53, p21 and caspase-3 gene expression levels were verified, nevertheless, in MCF-7 cells the mRNA level of the apoptosis-relevant p21 was elevated by 6-fold proving that apoptotic cell death signaling was induced in these breast cancer cells as well. Our results suggest that among the employed techniques electrophoretic deposition seems to be a suitable method to generate MnOx NPs that are adequate for future biomedical applications. Nevertheless, further structural and technical optimization as well as *in vitro* and *in vivo* screening of the antimicrobial efficiency and anticancer activity of these particles is recommended to evaluate their therapeutic potential.

5. Conclusions

A large body of evidence indicates that the synthesis method as well as the input material utilized to produce nanomaterials define substantially the physical and chemical properties and as a consequence, the biological activities of the obtained materials. The potential application, fate and behavior of nanoparticles particularly towards living systems relies on important functional properties such as size and shape, surface charge, biofunctional or catalytic activity. Careful considerations in the selection of the initial source material and the appropriate synthesis of the designed products ensures safety while maintaining nanoparticle function and efficiency. Therefore, in this study we aimed to carry out a comprehensive analysis to reveal how a naturally occurring mineral and the applied synthesis technique affect the physicochemical properties and as a result of these the antimicrobial and anticancer activities of manganese oxide nanoparticles to predict their attitude and performance on living cells. MnOx nanoparticles were successfully synthesized from the naturally occurring mineral pyrolusite

by various physical and chemical methods such as mechanical milling, electrophoretic deposition or vigorous stirring and precipitation. The as-prepared MnOx NPs were characterized using multiple techniques, which determined the exact composition, the crystalline structure, size and shape of the samples. The nanoparticles produced by electrophoretic deposition exhibited outstanding antifungal activity and proved to be effective against breast and prostate cancer cells, however they did not inhibit the growth of the tested Gram-positive and Gram-negative bacteria. The anticancer propensity of these manganese oxide nanoparticles was not the result of modulated cell proliferation or direct necrotic effect but was proven to be induced via apoptosis. Apoptosis induction by manganese containing nanoparticles was also verified by Yu et al., showing intracellular ROS generation, p53 activation, followed by an increase in bax levels, ultimately leading to G2/M arrest and increasing caspase-3 activity [35]. Apart from apoptosis, autophagy induction was also demonstrated in case of water-dispersible manganese oxide nanocrystals, where autophagy enhancement contributed to the synergistic effects between nanomaterials and chemotherapy agents in order to produce greater lethality against tumors [36].

Our results highlight that it is possible to produce MnOx NPs from this mineral, nevertheless, they also accentuate the importance of the proper nanoparticle synthesis method especially when the nanoparticles are aimed for biomedical applications. We demonstrate that manganese oxide nanoparticles suitable for antimicrobial and anticancer therapy can be obtained via an adequately chosen synthetic approach. We provide evidence and further emphasis to the potentials of MnOx NPs for pharmaceutical research and rational drug development and to be regarded as attractive candidates upon industrial considerations. In future experiments we plan to generate EM NPs with different physical and chemical properties by electrophoretic deposition to seek further structural optimization and we aim the obtained materials to an even more detailed *in vitro* screening to inspect their toxicity on numerous Gram-negative and -positive bacteria, on a number of fungal strains (such as Candida sp.), on various cancer cell lines and primary cancer cells. In case of favorable results, the performance of these particles should be evaluated in *in vivo* infection animal models (e.g. oral candidiasis model) and in xenograft mouse experiments.

CRediT authorship contribution statement

Ilona Pfeiffer: Methodology, Resources, Supervision, Writing – original draft, Writing – review & editing. **Mónika Kiricsi:** Conceptualization, Methodology, Project administration, Supervision, Writing – original draft, Writing – review & editing. **Zoltán Kónya:** Funding acquisition, Methodology, Resources, Supervision, Writing – original draft, Writing – review & editing. **Andrea Rónavári:** Conceptualization, Data curation, Formal analysis, Investigation, Methodology, Project administration, Validation, Writing – original draft. **Altantuya Ochirkhuyag:** Conceptualization, Investigation, Software. **Nóra Igaz:** Data curation, Formal analysis, Investigation, Software, Validation. **Bettina Szerencsés:** Data curation, Formal analysis, Investigation, Methodology, Validation. **Gergő Ballai:** Data curation, Formal analysis, Investigation, Visualization. **Ildikó Huliák:** Formal analysis, Investigation, Software. **Ákos Kovács:** Investigation, Software, Visualization. **Csenge Bocz:** Investigation, Software, Visualization.

Declaration of Competing Interest

The authors declare that they have no known competing financial interests or personal relationships that could have appeared to influence the work reported in this paper.

Data Availability

Data will be made available on request.

Acknowledgements

A.R. (BO/00384/21/7) and I.N. (Grant no. BO/00351/22/8) were supported by the János Bolyai Research Scholarship of the Hungarian Academy of Sciences and by the New National Excellence Program of the Ministry of Human Capacities of Hungary (ÚNKP-22–5-SZTE-583, ÚNKP-23–5 -SZTE-687 for A.R. and ÚNKP-22–5-SZTE-553 for I.N.) and by the University of Szeged IKIKK Horizontal Incubation Competence Centre. This research work was conducted with the support of the National Scientists Academy under the sponsorship of the Hungarian Ministry of Innovation and Technology (FEIF/646–4/2021-ITM_SZERZ) to C.B. and Á.K.

Appendix A. Supporting information

Supplementary data associated with this article can be found in the online version at doi:10.1016/j.colsurfa.2024.133528.

References

[1] M.J. Mitchell, M.M. Billingsley, R.M. Haley, M.E. Wechsler, N.A. Peppas, R. Langer, Engineering precision nanoparticles for drug delivery, Nat. Rev. Drug Discov. vol. 20 (2) (2021), https://doi.org/10.1038/s41573-020-0090-8.
[2] E. Sánchez-López, et al., Metal-based nanoparticles as antimicrobial agents: An overview, Nanomaterials vol. 10 (2) (2020), https://doi.org/10.3390/nano10020292.
[3] V. Chandrakala, V. Aruna, G. Angajala, Review on metal nanoparticles as nanocarriers: current challenges and perspectives in drug delivery systems, Emergent Mater. vol. 5 (6) (2022), https://doi.org/10.1007/s42247-021-00335-x.
[4] S. Manikandan, R. Subbaiya, M. Saravanan, H. Barabadi, R. Arulvel, Emerging Theragnostic Metal-Based Nanomaterials to Combat Cancer, *Nanotechnol. Life Sci.* (2021), https://doi.org/10.1007/978-3-030-74330-7_11.
[5] T.G. Agnihotri, S.S. Gomte, A. Jain, Emerging theranostics to combat cancer: a perspective on metal-based nanomaterials, Drug Dev. Ind. Pharm. vol. 48 (11) (2022), https://doi.org/10.1080/03639045.2022.2153862.
[6] B. Bahrami, et al., Nanoparticles and targeted drug delivery in cancer therapy, Immunol. Lett. vol. 190 (2017), https://doi.org/10.1016/j.imlet.2017.07.015.
[7] H. Sabit, et al., Nanocarriers: A Reliable Tool for the Delivery of Anticancer Drugs, Pharmaceutics vol. 14 (8) (2022), https://doi.org/10.3390/pharmaceutics14081566.
[8] M.S. Chavali, M.P. Nikolova, Metal oxide nanoparticles and their applications in nanotechnology, SN Appl. Sci. vol. 1 (6) (2019), https://doi.org/10.1007/s42452-019-0592-3.
[9] W.M. Saod, L.L. Hamid, N.J. Alaallah, A. Ramizy, Biosynthesis and antibacterial activity of manganese oxide nanoparticles prepared by green tea extract, Biotechnol. Rep. vol. 34 (2022), https://doi.org/10.1016/j.btre.2022.e00729.
[10] S.M. Dizaj, F. Lotfipour, M. Barzegar-Jalali, M.H. Zarrintan, K. Adibkia, Antimicrobial activity of the metals and metal oxide nanoparticles, Mater. Sci. Eng. C. vol. 44 (2014), https://doi.org/10.1016/j.msec.2014.08.031.
[11] Y.H. Leung, et al., Mechanisms of antibacterial activity of mgo: Non-ros mediated toxicity of mgo nanoparticles towards Escherichia coli, Small vol. 10 (6) (2014), https://doi.org/10.1002/smll.201302434.
[12] C. Zhu, et al., Manganese-based multifunctional nanoplatform for dual-modal imaging and synergistic therapy of breast cancer, Acta Biomater. vol. 141 (Mar. 2022) 429–439, https://doi.org/10.1016/J.ACTBIO.2022.01.019.
[13] K. Zhang, C. Qi, K. Cai, Manganese-based tumor immunotherapy, Adv. Mater. (2023), https://doi.org/10.1002/adma.202205409.
[14] B. Hernroth, I. Holm, A. Gondikas, H. Tassidis, "Manganese inhibits viability of prostate cancer cells, Anticancer Res vol. 38 (1) (2018), https://doi.org/10.21873/anticanres.12201.
[15] M.H. Cho, E.S. Choi, S. Kim, S.H. Goh, Y. Choi, Redox-responsive manganese dioxide nanoparticles for enhanced MR imaging and radiotherapy of lung cancer (no. DEC), Front Chem. vol. 5 (2017), https://doi.org/10.3389/fchem.2017.00109.
[16] Q. Ren, et al., Biodegradable hollow manganese/cobalt oxide nanoparticles for tumor theranostics, Nanoscale vol. 11 (47) (2019), https://doi.org/10.1039/c9nr07725a.
[17] J. Bauer, D.H. Buss, O. Glemser, The Electrochemical Behaviour of Manganese (II)-Hydroxide/Magnesium Hydroxide and Manganese (II)-Hydroxide/Calcium Hydroxide, Ber. der Bunsenges. F. üR. Phys. Chem. vol. 90 (9) (1986), https://doi.org/10.1002/bbpc.19860900910.
[18] N. Fairley, et al., Systematic and collaborative approach to problem solving using X-ray photoelectron spectroscopy, Appl. Surf. Sci. Adv. vol. 5 (2021), https://doi.org/10.1016/j.apsadv.2021.100112.
[19] M. Musil, B. Choi, A. Tsutsumi, Morphology and Electrochemical Properties of α-, β-, γ-, and δ-MnO 2 Synthesized by Redox Method, J. Electrochem Soc. vol. 162 (10) (2015), https://doi.org/10.1149/2.0201510jes.
[20] Y.N. Ko, S.Bin Park, S.H. Choi, Y.C. Kang, One-pot synthesis of manganese oxide-carbon composite microspheres with three dimensional channels for Li-ion batteries, Sci. Rep. vol. 4 (2014), https://doi.org/10.1038/srep05751.

[21] T. Gao, H. Fjellvåg, P. Norby, A comparison study on Raman scattering properties of α- and β-MnO2, Anal. Chim. Acta vol. 648 (2) (2009), https://doi.org/10.1016/j.aca.2009.06.059.
[22] H.U. Shah, et al., Electrochemical Properties of Controlled Size Mn 3 O 4 Nanoparticles for Supercapacitor Applications, J. Nanosci. Nanotechnol. vol. 18 (1) (2017), https://doi.org/10.1166/jnn.2018.14644.
[23] F. Buciuman, F. Patcas, R. Craciun, D.R.T. Zahn, Vibrational spectroscopy of bulk and supported manganese oxides, Phys. Chem. Chem. Phys. vol. 1 (1) (1999), https://doi.org/10.1039/a807821a.
[24] Y. Luo, J. Ding, Y. Shen, W. Tan, G. Qiu, F. Liu, Symbiosis mechanism of iron and manganese oxides in oxic aqueous systems, Chem. Geol. vol. 488 (2018), https://doi.org/10.1016/j.chemgeo.2018.04.030.
[25] C.R. Kalaiselvan, S.S. Laha, S.B. Somvanshi, T.A. Tabish, N.D. Thorat, N.K. Sahu, Manganese ferrite (MnFe2O4) nanostructures for cancer theranostics, Coord. Chem. Rev. vol. 473 (2022), https://doi.org/10.1016/j.ccr.2022.214809.
[26] Z. Yang, et al., Probing the Release and Uptake of Water in a-MnO2·xH2O,", Chem. Mater. vol. 29 (4) (2017) https://doi.org/10.1021/acs.chemmater.6b03721.
[27] M.C. Biesinger, B.P. Payne, A.P. Grosvenor, L.W.M. Lau, A.R. Gerson, R.S.C. Smart, Resolving surface chemical states in XPS analysis of first row transition metals, oxides and hydroxides: Cr, Mn, Fe, Co and Ni, Appl. Surf. Sci. vol. 257 (7) (2011), https://doi.org/10.1016/j.apsusc.2010.10.051.
[28] B. Ding, P. Zheng, P. Ma, J. Lin, Manganese Oxide Nanomaterials: Synthesis, Properties, and Theranostic Applications, Adv. Mater. vol. 32 (10) (2020), https://doi.org/10.1002/adma.201905823.
[29] A. Haleem, M. Javaid, R.P. Singh, S. Rab, R. Suman, Applications of nanotechnology in medical field: a brief review, Glob. Health J. vol. 7 (2) (Jun. 2023) 70–77, https://doi.org/10.1016/J.GLOHJ.2023.02.008.
[30] N. Baig, I. Kammakakam, W. Falath, I. Kammakakam, Nanomaterials: A review of synthesis methods, properties, recent progress, and challenges, Mater. Adv. vol. 2 (6) (2021), https://doi.org/10.1039/d0ma00807a.
[31] G. Yang, J. Ji, Z. Liu, "Multifunctional MnO2 nanoparticles for tumor microenvironment modulation and cancer therapy," *Wiley Interdisciplinary Reviews: Nanomedicine and Nanobiotechnology*, no vol. 13 (6) (2021), https://doi.org/10.1002/wnan.1720.
[32] A. Rónavári, et al., Multi-round recycling of green waste for the production of iron nanoparticles: synthesis, characterization, and prospects in remediation, Discov. Nano vol. 18 (1) (2023), https://doi.org/10.1186/s11671-023-03784-x.
[33] A. Rónavári, et al., Biological activity of green-synthesized silver nanoparticles depends on the applied natural extracts: A comprehensive study, Int J. Nanomed. vol. 12 (2017), https://doi.org/10.2147/IJN.S122842.
[34] X. Jiang, P. Gray, M. Patel, J. Zheng, J.J. Yin, Crossover between anti- And pro-oxidant activities of different manganese oxide nanoparticles and their biological implications, J. Mater. Chem. B vol. 8 (6) (2020), https://doi.org/10.1039/c9tb02524c.
[35] C. Yu, et al., In depth analysis of apoptosis induced by silica coated manganese oxide nanoparticles in vitro, J. Hazard Mater. vol. 283 (2015), https://doi.org/10.1016/j.jhazmat.2014.09.060.
[36] Y. Lu, et al., MnO nanocrystals: A platform for integration of MRI and genuine autophagy induction for chemotherapy, Adv. Funct. Mater. vol. 23 (12) (2013), https://doi.org/10.1002/adfm.201202233.